Optics Communications 523 (2022) 128735

Contents lists available at ScienceDirect

Optics Communications

journal homepage: www.elsevier.com/locate/optcom

Characterization of fiber modal impairments using direct-detection methods

Mahmoudreza Dadras [a,*], Ioannis Roudas [a], Jaroslaw Kwapisz [b]

[a] Department of Electrical and Computer Engineering, Montana State University, Bozeman, MT 59717, United States
[b] Department of Mathematical Sciences, Montana State University, Bozeman, MT 59717, United States

ARTICLE INFO

Keywords:
Multimode fiber characterization
Modal dispersion
Mode-dependent loss

ABSTRACT

The mode-dependent signal delay and average power methods are inexpensive direct-detection techniques that can be utilized to characterize the modal dispersion and the mode-dependent loss of multimode and multicore optical fibers. In this paper, we study by simulation the impact of receiver noise, device imperfections, and implementation penalties on the accuracy of these methods in the case of few-mode fibers. We show that there is a set of optimal launch modes that can minimize errors in the estimation of modal dispersion and mode-dependent loss.

1. Introduction

Space division multiplexing (SDM), in conjunction with multimode fibers (MMFs) or multicore fibers (MCFs), can increase the link capacity [1]. Different spatial paths provided by different modes/cores can be utilized for independent data stream transmission through the fiber [2]. However, transmission impairments in MMFs and MCFs, such as modal dispersion (MD), mode-dependent loss (MDL), and intermodal/intercore coupling, should be taken into account in the design of a reliable and efficient multiple-input multiple-output (MIMO) system.

MD is the dominant limiting factor in uncompensated MMF links since it causes strong intersymbol interference (ISI) at the optical receiver [3,4], and must be thoroughly characterized. The formalism of polarization mode dispersion (PMD) in single-mode fibers (SMFs) can be generalized to describe MD in MMFs. More specifically, MD can be described by the principal modes (PMs) and their corresponding differential mode group delays (DMGDs), which are jointly represented by a vector in a generalized Stokes space, the so-called MD vector [5].

To measure the MD of MMFs, several methods have been proposed in the optical communications literature [6–9]. For instance, Carpenter et al. [9] used swept wavelength interferometry (SWI) to measure the fiber transfer matrix. This method requires a coherent optical receiver and can provide information about PMs, DMGDs, and MDL of the fiber under test at once. This is because it is based on amplitude and phase measurements of input and output modes that can be used to infer the fiber transfer matrix.

A new method that can fully characterize the MD of an MMF is the mode-dependent signal delay method (MD-SDM) [10]. This is a generalization of the polarization-dependent signal delay method (PD-SDM) for the measurement of the PMD vector in SMFs [11]. In this method, the time-of-flight of optical pulses is utilized to characterize the MD of the fiber, which can be done using a direct-detection receiver. It was analytically shown [10,12] that the input MD vector components can be determined by such group delay measurements. Once the input MD vector is known, the input group-delay operator can be constructed and the input MD and DMGDs can be estimated [12]. Similarly, for MDL characterization, one can determine the MDL vector by launching optical pulses and measuring their average output powers. We will refer to this characterization technique as the mode-dependent average power method (MD-APM).

In this paper, we use Monte Carlo simulation to study the accuracy of the MD-SDM and the MD-APM for fiber characterization, which has not been addressed before (although early simulation results were presented in [13]). We use optimized launch modes to minimize the noise error in the estimation of the MD and MDL vectors [12,14]. We show that, for different fibers, the DMGDs and input PMs of the fiber can be estimated by using the MD-SDM. For instance, for a given 500-m-long 6-mode fiber, we observe that the difference between the magnitude of the MD vector measured using the MD-SDM and estimated directly from the fiber transfer matrix in the absence of the MDL is only 1.22 ps. The MDL vector of the fiber can also be determined using the MD-APM by measuring the average output power of optical pulses. In addition, we measure the MD vector and the MDL of the fiber in different coupling regimes. The MD vector is estimated for different few-mode fiber (FMF) lengths as well. We demonstrate that the maximum discrepancy in the magnitude of the MD vector with and without the MDL is less than 1.6 ps. Furthermore, we investigate the impact of the thermal noise of the direct-detection receiver and the modal crosstalk introduced by the mode converter at the FMF input on MD vector characterization. Finally, the impact of various sets of launch vectors on the accuracy of the MD and MDL vectors estimation is analyzed. We show that using

* Corresponding author.
E-mail address: mdadras@montana.edu (M. Dadras).

https://doi.org/10.1016/j.optcom.2022.128735
Received 4 January 2022; Received in revised form 28 May 2022; Accepted 2 July 2022
Available online 8 July 2022

the optimal launch vectors proposed in [12] reduces the penalty in MD vector and MDL estimations by 3.22 dB and 4.11 dB, respectively, compared to the random launch vectors.

2. Operating principle overview

2.1. Modal dispersion

Initially, we consider the ideal case of an MMF without MDL, i.e, the fiber transfer matrix $\mathbf{U}(\omega)$ is unitary. The input group-delay operator is defined as $\imath\mathbf{U}^{\dagger}(\omega)\mathbf{U}_{\omega}(\omega)$ [5,12], where the subscript ω in $\mathbf{U}_{\omega}(\omega)$ denotes differentiation with respect to the angular frequency and the dagger denotes the adjoint matrix. The input group-delay operator can be expressed in terms of the identity matrix $\mathbf{I}$ and the generalized Gell-Mann matrices, $\boldsymbol{\Lambda} := \left[\boldsymbol{\Lambda}_1, \ldots, \boldsymbol{\Lambda}_{N^2-1}\right]^T$, where N is the number of modes and T indicates transposition [12]

$$\imath\mathbf{U}^{\dagger}(\omega)\mathbf{U}_{\omega}(\omega) := \tau_0(\omega)\mathbf{I} + \frac{1}{2C_N}\vec{\tau}_s(\omega)\cdot\boldsymbol{\Lambda}. \tag{1}$$

In (1), $\tau_0(\omega)$ represents the average group delay in the MMF under test, $\vec{\tau}_s$ is the input MD vector in the generalized Stokes space, and C_N is a normalization coefficient defined as $C_N := \sqrt{N/[2(N-1)]}$.

The MD-SDM [12] can be used to characterize the DMGDs and input PMs of the fiber. The eigenvalues and the eigenvectors of the input group-delay operator are the DMGDs and the input PMs, respectively. The group delay τ_g of an optical pulse is related to the input MD vector $\vec{\tau}_s$ and the combination of launch modes, which is represented by Stokes vector $\hat{s}$, as follows [12]

$$\tau_g = \tau_0 + \frac{1}{2C_N^2}\left\langle\vec{\tau}_s\right\rangle\cdot\hat{s}, \tag{2}$$

where $\langle\cdot\rangle$ denotes spectral averaging.

In (2), τ_g is defined as the time average [12]

$$\tau_g := \frac{\int_{-\infty}^{\infty} tP(t)dt}{\int_{-\infty}^{\infty} P(t)}dt, \tag{3}$$

where $P(t)$ denotes the instantaneous optical power at the fiber output.

In the beginning, we can estimate the average group-delay τ_0 by launching N pulses corresponding to N arbitrary orthogonal launch states in Jones space. For instance, we can use the MMF eigenmodes, i.e., we can launch first all the power at the fundamental mode LP_{01} in the x-polarization; next, we can launch all the transmitted power at the LP_{01} mode in the y-polarization; and so forth. Then, the average group delay is calculated by averaging the delays of the different eigenmodes. Next, we employ (2) to form a $(N^2-1)\times(N^2-1)$ matrix. To calculate this matrix, first, we need to define the coefficient matrix

$$\mathbf{S} = \left[\hat{s}_1, \ldots, \hat{s}_{N^2-1}\right]^T, \tag{4}$$

where columns contain the N^2-1 launch states, corresponding to the linearly independent Stokes vectors $\hat{s}_i$, $i = 1, 2, \ldots, N^2-1$. Afterwards, we use N^2-1 optimal launch states corresponding to different fiber spatial mode combinations. For every launch state, we measure the power of output pulses using direct detection and calculate the group delays using (3). Finally, a set of equations can be formed using (2) [12], and, the MD vector $\vec{\tau}_s$ can be estimated by matrix inversion [12].

2.2. Mode-dependent loss

In practice, MDL is always present in MMFs and must be characterized first because it impacts the MD measurement described in Section 2.1. MDL is the combined result of differences in the attenuation coefficients of different modes and of coupling among various modes due to manufacturing imperfections, fiber bends, and other mechanical deformations [12]. In [12], the authors proposed a variant of the MD-SDM, called the MD-APM, to characterize the MDL before MD.

If MDL is not negligible, the transfer matrix of the multimode fiber is not unitary and is denoted by $\mathbf{H}(\omega)$. In this case, the input group-delay operator is defined as $\imath\mathbf{H}_{\omega}(\omega)\mathbf{H}^{-1}(\omega)$ [12]. This is a non-Hermitian matrix with complex eigenvalues and non-orthogonal eigenvectors. To characterize MDL, as indicated in [12], we can express $\mathbf{H}(\omega)$ as a product of a unitary matrix $\mathbf{U}(\omega)$ and a positive definite matrix $\mathbf{P}(\omega)$. The MDL is the ratio of the maximum and minimum of the eigenvalues of the positive definite matrix $\mathbf{P}(\omega)^2$. The latter can be written as

$$\mathbf{P}(\omega)^2 = \alpha_0(\omega)\left[\mathbf{I} + \frac{1}{2C_N}\vec{\Gamma}(\omega)\cdot\boldsymbol{\Lambda}\right], \tag{5}$$

where $\alpha_0(\omega)$ denotes the mean attenuation of the fiber and $\vec{\Gamma}(\omega)$ is the MDL vector [12]. Due to the similarity between Eqs. (5) and (1), we follow a similar procedure to the one described in Section 2.1.

For MDL characterization, first, we launch N orthogonal modes in Jones space into the MMF and measure the output powers corresponding to these launched pulses. Averaging over the output powers P_k and normalizing with the input power P_{In} gives the estimated mean attenuation of the fiber

$$\alpha_0(\omega) = \frac{1}{NP_{\mathrm{In}}}\sum_{k=1}^{N} P_k. \tag{6}$$

Next, we launch N^2-1 mode combinations, which are independent in the Stokes space, and measure the corresponding output powers P_{g_i}, $i = 1, 2, \ldots, N^2-1$. The matrix representation of the system of equations can be written as $\mathbf{S}\vec{\Gamma}(\omega) = \Delta\alpha$, where $\Delta\alpha = \left[\Delta\alpha_1, \ldots \Delta\alpha_{N^2-1}\right]^T$ is a vector with elements $\Delta\alpha_i := \alpha_i - \alpha_0$ and α_i is defined as $\alpha_i := P_{g_i}/P_{\mathrm{In}}$. Therefore, the MDL vector can be determined by solving the matrix equation

$$\vec{\Gamma}(\omega) = \mathbf{S}^{-1}\Delta\alpha. \tag{7}$$

In addition, since $\mathbf{P}(\omega)$ is known, we can pre-compensate for MDL and calculate the transfer matrix of the compensated optical fiber using the method in Section 2.1. In other words, we construct new mode combinations for the pre-compensation using the formula

$$|s_k'\rangle = \mathbf{P}(\omega)^{-1}|s_k\rangle, \tag{8}$$

where $|s_k\rangle$ and $|s_k'\rangle$ denote the uncompensated and pre-compensated launch states, respectively. After calculation of the pre-compensated launch states, the corresponding mean group-delay, $\tau_0'(\omega)$, and the MD vector, $\vec{\tau}_s'(\omega)$, can be calculated by the procedure described in Section 2.1. Therefore, the compensated input group-delay operator and input group-delay operator of the fiber in the presence of MDL can be determined [12]. Subsequently, the MD vector in the presence of the MDL is complex and can be calculated by

$$\vec{\tau}_s'(\omega) := C_N\mathrm{Tr}[\imath\mathbf{H}^{-1}(\omega)\mathbf{H}_{\omega}(\omega)\cdot\boldsymbol{\Lambda}], \tag{9}$$

where Tr(.) denotes the trace of a matrix.

To summarize, first, the MD-APM can be used to characterize MDL and, subsequently, the MD-SDM can be used to characterize MD. In the joint presence of MD and MDL, initially, we characterize the MDL using the MDL formalism described in Section 2.2 and then perform MD vector measurement of the compensated fiber transfer matrix. Finally, we create the non-Hermitian input group delay operator for estimating the MD vector.

2.3. Modal crosstalk at the launch

Both the MD-SDM and MD-APM depend on the accuracy of selecting mode combinations. Indeed, modal crosstalk on the transmitter side is one of the most important limiting factors of the method and it can be minimized by utilizing optimal launch vectors in the Stokes space [12,15]. For instance, if a spatial light modulator (SLM) is used as mode converter, it is possible to optimize the phase mask to reduce the crosstalk. However, even a small amount of crosstalk can affect the measurement of the input MD vector. In this section, we present a high-level model of modal crosstalk for different numbers of modes.

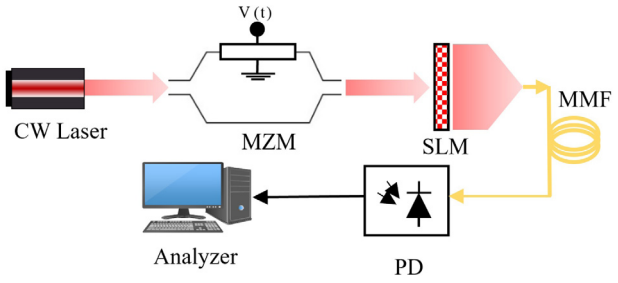

Fig. 1. Simulation setup for MMF characterization using the MD-SDM (Abbreviations: CW: Continuous Wave, V(t): Bias voltage, MZM: Mach–Zehnder modulator, SLM: Spatial light modulator, MMF: Multimode fiber, PD: Photodetector).

In order to model the modal crosstalk introduced by the mode converter without taking into account the device physics, we assume that we launch unintentionally a vector $|s'_k\rangle$, instead of the desired mode combination $|s_k\rangle$ [12]. In simulation, we use an abstract procedure to generate the input vectors $|s'_k\rangle$. First, we generate a random vector and then find the orthonormal component $|\Delta s\rangle$ of this vector with respect to $|s_k\rangle$. The perturbed vector $|s'_k\rangle$ can be expressed as $|s'_k\rangle = \sqrt{1-\varepsilon}|s_k\rangle + \sqrt{\varepsilon}|\Delta s\rangle$, where ε denotes the modal crosstalk level.

2.4. Thermal noise

Thermal noise is the most significant source of noise in direct-detection optical receivers. As indicated in [12], the variance of the measured length of the MD vector due to thermal noise in the direct-detection receiver can be estimated by

$$\sigma^2_{\delta\tau_g} = \mathrm{Tr}\left[\mathbf{A}\mathbf{A}^T\right]\frac{N_0 C_N^4 T^3}{6R_d^2\bar{E}^2}, \tag{10}$$

where $\mathbf{A} = \mathbf{S}^{-1}$. In (10), N_0, T, R_d, and $\bar{E}$ denote the power spectral density (PSD) of the thermal noise, the integration time for the computation of the group delays, the responsivity of the photodiode, and the average energy of the received pulse, respectively. Then, we calculate a bound of the relative error in the MD vector by

$$B_{RE} := \frac{\sigma_{\delta\tau_g}}{\|\vec{\tau}_s\|}, \tag{11}$$

where $\sigma_{\delta\tau_g}$ denotes the standard deviation of the thermal noise in the receiver.

3. Simulation of MD-SDM and MD-APM

Using the simulation setup shown in Fig. 1, we studied the propagation of light through various FMFs. For this simulation, we used graded-index FMFs with parabolic refractive index profile for the fiber core. The waveform is generated by a continuous wave (CW) laser and modulated by a Mach–Zehnder modulator (MZM). Then, the SLM is used to provide different mode combinations to propagate through the FMF. At the output of the FMF, optical pulses are detected by a photodetector and the PMs and DMGDs are estimated by processing the results in a personal computer. For simplicity, we assume idealized, chirp-free, narrowband Gaussian optical pulses.

Table 1 shows the parameters that were used in the simulation.

To simulate real fibers, we consider different properties of FMFs that cause different modes to have different group delays. Delays due to the polarization and spatial configurations of the LP modes are simulated by taking into account the mode dispersion and intramode group delay parameters. In addition, we enabled mode coupling as well to consider intragroup coupling. Every couple of hundred meters, strong coupling may occur due to the similarity of the propagation constant, resulting in full coupling of the modes. Therefore, we consider mean section length and all mode correlation length to consider this effect. Finally, to be more accurate, we also include standard deviation of the mean section length.

Table 1
Simulation parameters.

Parameter	Value	Unit
Fiber length	1–20,000	m
Group refractive index	1.47	–
Attenuation	0.2–0.6	dB/km
Refractive index reference frequency	193.1	THz
Core refractive index	1.45	–
Index contrast	0.02	–
Core diameter	10–18	μm
Cladding diameter	125	μm
Connector efficiency	64	%
Optical loss at connectors	2	dB
PMD coefficient	1.58×10^{-15}	$\sqrt{s/m}$
PMD correlation length	150	m
Correlation length	130	m
All modes correlation length	130	m
Effective area LP_{01}	80	μm^2
Mean section length	500	m
Section length deviation	5	m
Photodiode responsivity	1	A/W
Photodiode thermal noise	10^{-9}–10^{-12}	$A/\sqrt{Hz}$

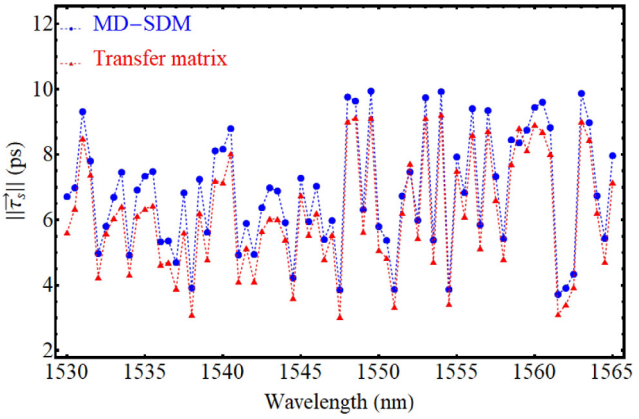

Fig. 2. MD vector estimation in the absence of MDL using the MD-SDM (blue) and the fiber transfer matrix (red).

4. Results and discussion

In this section, we present simulation results for the characterization of different fibers using the MD-SDM and the MD-APM. The accuracy in estimating the norm of the MD vector has been utilized as a figure of merit for the proper operation of the MD-SDM. Fig. 2 compares the magnitude of the MD vector as a function of wavelength derived from the transfer matrix (red) and estimated using the MD-SDM (in blue) without MDL, for a 500 m long 6-mode fiber. We observe that there is a small discrepancy between the MD vector estimates using the two methods. Specifically, we note that the largest difference is 1.22 ps, which occurs at 1537.5 nm in the C-band.

When the fiber has MDL, the transfer matrix of the fiber is not unitary and we calculate the MD vector using the process in Section 2.2. Fig. 3 shows the MD vector estimation using the process in Section 2.1 after we compensate the MDL as described in 2.2. As expected, the MD estimation error is larger now. The maximum error is 3.41 ps and occurs at 1552.5 nm.

MDL plays a fundamental role for limiting the signal propagation in SDM fibers. As mentioned above, the presence of the MDL affects on the MD vector characterization and, therefore, MDL estimation is vital in using MD-SDM. In addition, we can calculate the transfer matrix of the fiber using input and output PMs, which is provided by the simulation tool. The transfer matrix can be calculated using $\mathbf{H}(\omega) = \mathbf{PM}_{\mathrm{Out}}(\omega)\mathbf{PM}_{\mathrm{In}}(\omega)^{-1}$, and then MDL can be estimated by the ratio of the largest eigenvalue to the smallest eigenvalue of the $\mathbf{P}(\omega)^2 = \mathbf{H}(\omega)^{\dagger}\mathbf{H}(\omega)$ [12].

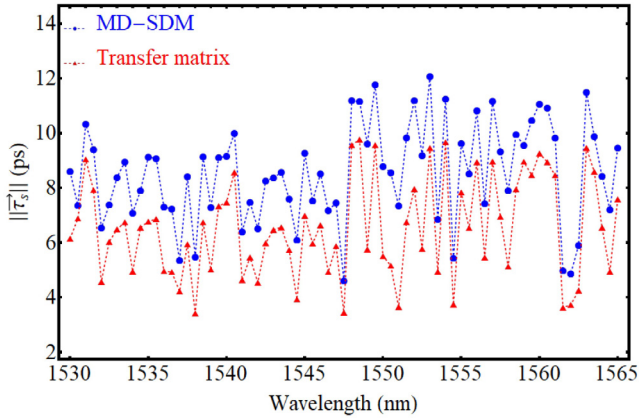

Fig. 3. MD vector estimation in the presence of MDL using the MD-SDM (blue) and the fiber transfer matrix (red).

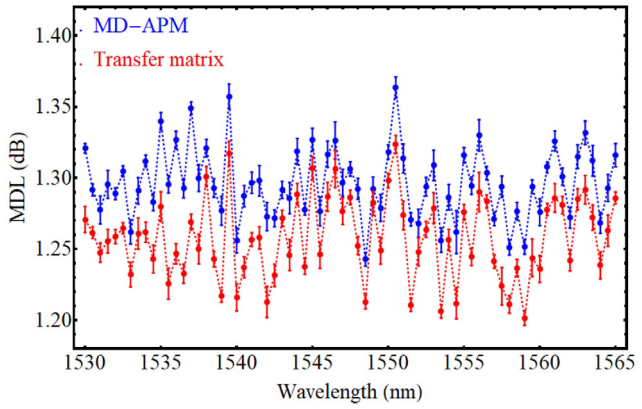

Fig. 4. Comparison of the estimated MDL by the MD-APM (blue) and the MDL derived by the transfer matrix (red).

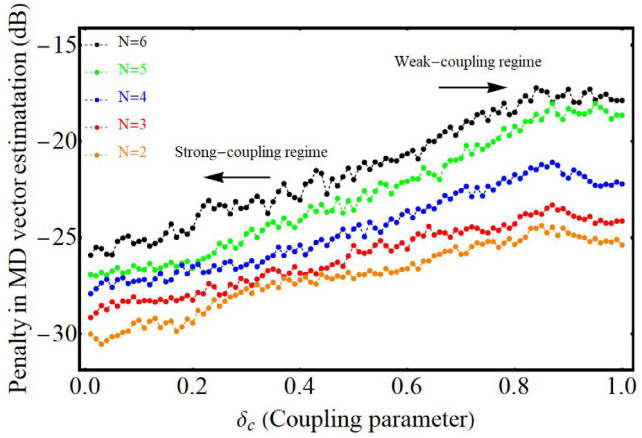

Fig. 5. Penalty in MD vector estimation as a function of the coupling parameter (Symbols: Orange: N=2, Red: N=3, Blue: N=4, Green: N=5, Black: N=6).

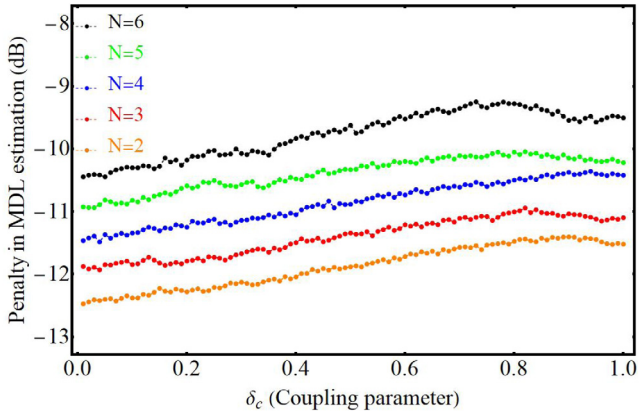

Fig. 6. Penalty in MDL estimation as a function of the coupling parameter (Symbols: Orange: N=2, Red: N=3, Blue: N=4, Green: N=5, Black: N=6).

Fig. 4 shows the MDL and the effect of the receiver thermal noise in the MDL measurement in the C-band from the transfer matrix and the MD-APM. In addition, we used vertical error bars to show the means and associated spread in the MDL measurements. In fact, each time we ran the simulation in the C-band, we observed different MDL due to the receiver thermal noise, and we considered the maximum error to plot the spread of the MDL measurement. For example, at 1536 nm, there is a 0.1 dB deviation between the estimated value and the actual MDL of a 500 m 6-mode fiber.

Mode coupling in MMFs is another factor that affects the performance of a transmission system. Here, we estimate the accuracy of the MD-SDM and the MD-APM at different coupling regimes. We define the coupling parameter as [16] $\delta_c := L_c/L_s$, where L_c and L_s denote the correlation length and the fiber length, respectively. When δ_c is close to one we are in the weak-coupling regime. When δ_c approaches zero, the correlation length is much shorter than the system length, and we are in the strong-coupling regime. We defined the penalty in MD vector estimation as $10log(\|\vec{\tau}_s\|_{MD-SDM} - \|\vec{\tau}_s\|_{TM})/\|\vec{\tau}_s\|_{TM}$, where $\|\vec{\tau}_s\|_{MD-SDM}$ and $\|\vec{\tau}_s\|_{TM}$ denoted the MD vector from the MD-SDM and fiber transfer matrix, respectively. For the MDL estimation, we defined the penalty as $10log(\mathrm{MDL}_{MD-APM} - \mathrm{MDL}_{TM})/\mathrm{MDL}_{TM}$.

Fig. 5 shows the impact of different coupling regimes on the MD vector estimation using the MD-SDM. Strong coupling reduces the separation of group delays and it can compensate for MD vector estimation errors. For example, for a 1 km 6-mode fiber, the penalty for using this method compared to using the fiber transfer matrix for the MD vector estimation is less than −25 dB.

Fig. 6 shows the penalty in MDL estimation for different coupling regimes. Similar to the MD vector estimation, the penalty in MDL estimation decreases slightly when we approach to the strong-coupling regime.

Next, we compute the norm of the MD vector for different numbers of modes and different fiber lengths to illustrate the impact of the MDL on the MD characterization. We adjusted the correlation length and fiber length to make the coupling parameter δ_c at 0.2 to be at the relatively strong coupling regime.

Fig. 7 shows the increase of the norm of the MD vector as a function of the fiber length for different numbers of modes in the absence and presence of the MDL. As shown, in the joint presence of MD and MDL, MDL induces progressively larger penalties in the MD vector estimation as the fiber length increases. For instance, for a 20 km long 6-mode fiber, the measured MD has an extra 1.6 ps of error compared to the measurement in absence of MDL.

The principal attenuation of the fiber determines the MDL of the fiber. It is accumulated along with the fiber, and depends on the number of modes and the coupling regime [17]. According to the chosen coupling parameter for our simulation, the MDL trend for different fiber lengths shows a growth roughly somewhere between a square root of the distance and the linear growth. In fact, the coupling strength can determine the MDL trend, and we can expect more linear growth by increasing the coupling parameter. Fig. 8 illustrates the MDL of the fiber as a function of the fiber length for different numbers of modes. For instance, for a 6-mode fiber, the MDL increases by 0.0625 dB on average for every 1 km of the fiber.

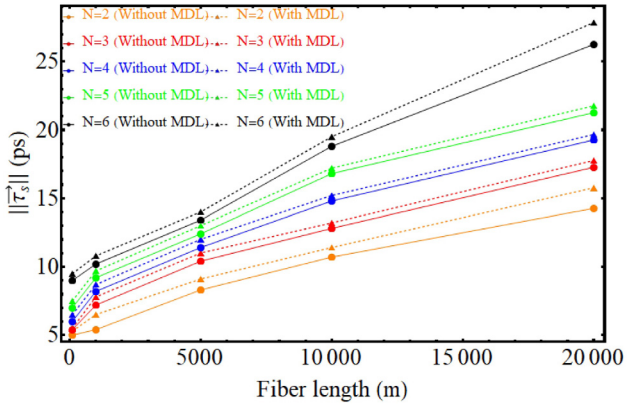

Fig. 7. The magnitude of the MD vector vs. fiber length for different numbers of modes in the absence and presence of MDL.

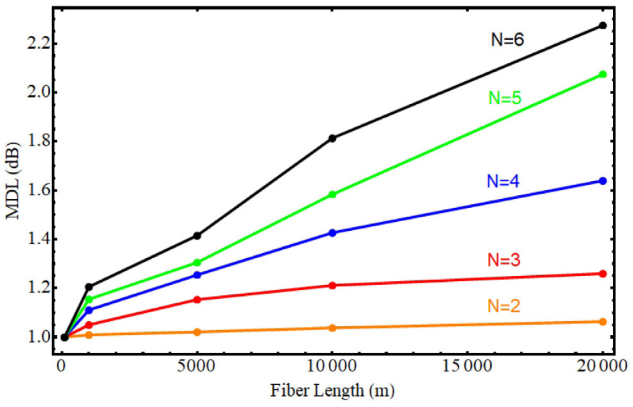

Fig. 8. MDL vs. fiber length for different numbers of modes (Symbols: Orange: = 2, Red: = 3, Blue: = 4, Green: = 5, Black: = 6).

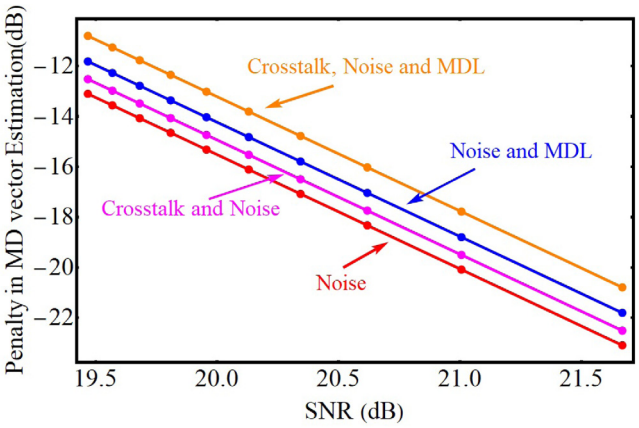

Fig. 9. Penalty in MD vector estimate as a function of the SNR in the presence of different sources of errors (Symbols: Red: Impact of noise, Magenta: Impact of crosstalk and noise, Blue: Impact of noise and MDL, Orange: Impact of crosstalk, Noise, and MDL for a two-mode fiber).

To further investigate the accuracy of the method, we consider other possible limitations like modal crosstalk and thermal noise along with the MDL, and their combined impacts on the performance of the channel. The penalty in MD vector estimation as a function of the SNR for different sources of errors is reported in Fig. 9. In this figure, all sources of errors, such as thermal noise at the direct-detection receiver, MDL as the transmission effect of the fiber, and error of the mode

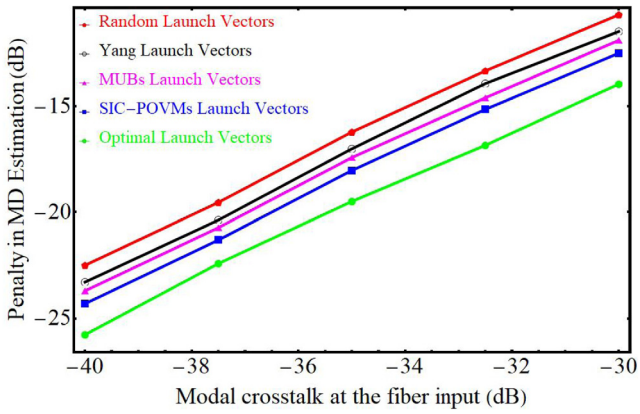

Fig. 10. Penalty in MD vector estimate as a function of modal crosstalk at the fiber input for different launch vectors (Symbols: Red: Random launch vectors, Black: Yang and Nolan's vectors [18], Magenta: MUBs launch vectors [19], Blue: SIC-POVMs launch vectors [20], Green: Optimal launch vectors [12]).

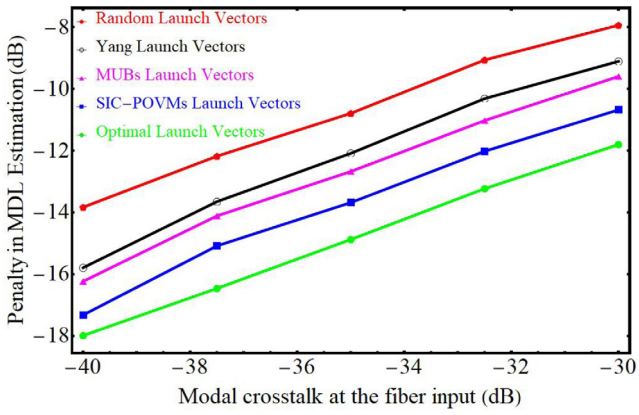

Fig. 11. Penalty in MDL estimation as a function of modal crosstalk at the fiber input for different launch vectors (Symbols: Red: Random launch vectors, Black: Yang and Nolan's vectors [18], Magenta: MUBs launch vectors [19], Blue: SIC-POVMs launch vectors [20], Green: Optimal launch vectors).

combiner are taken into account to show the accuracy of the MD-SDM and the MD-APM. For the parameter values used in our simulations, MDL leads to a higher penalty compared to crosstalk. In the presence of thermal noise, the MDL and the crosstalk penalties are compounded.

Using optimal launch vectors can minimize the error in the MD vector estimation. Fig. 10 compares different input launch vectors, such as Yang and Nolan's vectors [18], mutually unbiased bases (MUBs) [19], symmetric, informationally complete, positive operator valued measure (SIC-POVM) vectors [20], and the optimal launch vectors proposed in [12]. We observe that the optimal launch vectors [12] produce less penalty compared to other vector sets that were previously proposed. For instance, in a 6-mode fiber, the penalty in the MD estimation is decreased by 3.22 dB using optimal launch vectors instead of using random launch vectors when the modal crosstalk at the fiber input is −30 dB.

Fig. 11 illustrates the effect of using different launch vectors for the MDL measurement as a function of modal crosstalk. As expected, optimal launch vectors [12] can minimize the error in MDL estimation. In fact, the optimal launch vectors can reduce the penalty by 4.11 dB compared to random launch vectors when the modal crosstalk at the fiber input is −40 dB.

5. Conclusion

In this paper, we investigated the accuracy of the MD-SDM and the MD-APM in the characterization of FMFs. We simulated different

sources of errors and studied their impact on the accuracy of the MD-SDM and MD-APM. In addition, the MD and MDL of the fiber were investigated for different coupling regimes. Furthermore, the thermal noise of the direct-detection receiver and the modal crosstalk at the fiber input were discussed as two limiting factors in the MD vector estimation. Finally, we showed that using the optimal launch vectors could reduce the penalty in MD and MDL characterization. Experimental results for these measurement methods will be presented in future publications.

Declaration of competing interest

The authors declare the following financial interests/personal relationships which may be considered as potential competing interests: Ioannis Roudas reports financial support was provided by National Science Foundation.

Acknowledgments

This material is based upon work supported by the National Science Foundation under Grant No. 1911183 and Grant No. 1809043.

References

[1] D.J. Richardson, J.M. Fini, L.E. Nelson, Space-division multiplexing in optical fibres, Nat. Photonics 7 (5) (2013) 354–362.
[2] P.J. Winzer, R. Ryf, S. Randel, Spatial multiplexing using multipleinput multiple-output signal processing, in: Optical Fiber Telecommunications VIB, Academic, New York, NY, USA, 2013, ch. 10.
[3] K.-P. Ho, J.M. Kahn, Mode coupling and its impact on spatially multiplexed systems, in: I.P. Kaminow, T. Li, A.E. Willner (Eds.), Optical Fiber Telecommunications VI, Elsevier, 2013.
[4] C. Antonelli, A. Mecozzi, M. Shtaif, P.J. Winzer, Stokes-space analysis of modal dispersion in fibers with multiple mode transmission, Opt. Express 20 (2012) 11718–11733.
[5] I. Roudas, J. Kwapisz, Stokes space representation of modal dispersion, IEEE Photonics J. 9 (5) (2017) 1–15, Oct.
[6] T. Ahn, S. Moon, S. Kim, K. Oh, D.Y. Kim, J. Kobelke, K. Schuster, J. Kirchhof, Optical frequency-domain modal dispersion measurement in multimode fibers using intermodal interferometer, in: Optical Fiber Communication Conference (Paper OWI17), Anaheim, CA, 2006.
[7] J.W. Nicholson, A.D. Yablon, S. Ramachandran, S. Ghalmi, Spatially and spectrally resolved imaging of modal content in large-mode-area fibers, Opt. Express 16 (2008) 7233–7243.
[8] J. Demas, R. Siddharth, Sub-second mode measurement of fibers using C2 imaging, Opt. Express 22 (19) (2014) 23043–23056.
[9] J. Carpenter, B.J. Eggleton, J. Schröder, Observation of Eisenbud–Wigner–Smith states as principal modes in multimode fiber, Nat. Photonics 9 (11) (2015) 751–757.
[10] G. Milione, D.A. Nolan, R.R. Alfano, Determining principal modes in a multimode optical fiber using the mode dependent signal delay method, J. Opt. Soc. Amer. B, Opt. Phys. 32 (2015) 143–149.
[11] L.E. Nelson, R.M. Jopson, H. Kogelnik, J.P. Gordon, Measurement of polarization mode dispersion vectors using the polarization-dependent signal delay method, Opt. Express 6 (8) (2000) 158–167.
[12] I. Roudas, J. Kwapisz, D.A. Nolan, Optimal launch states for the measurement of principal modes in optical fibers, J. Lightwave Technol. 36 (20) (2018) 4915–4931, 15 Oct.
[13] M.R. Dadras, I. Roudas, J. Kwapisz, MD and MDL characterization using direct-detection pulse peasurements, in: IEEE Photonics Conference, IPC, Vancouver, BC, Canada, 2020.
[14] M.R. Dadras, I. Roudas, J. Kwapisz, Mode selection for measuring modal dispersion in Stokes space, in: IEEE Photonics Conference, IPC, Reston, VA, 2018.
[15] J.M. Gené, P.J. Winzer, A universal specification for multicore fiber crosstalk, IEEE Photonics Technol. Lett. 31 (9) (2019) 673–676.
[16] J.M. Kahn, K. Ho, M.B. Shemirani, Mode coupling effects in multi-mode fibers, in: Optical Fiber Communication Conference (Paper OW3D-3), Los Angeles, CA, 2012.
[17] K. Ho, Exact model for mode-dependent gains and losses in multimode fiber, J. Lightwave Technol. 30 (23) (2012) 3603–3609.
[18] J. Yang, D.A. Nolan, Using state tomography for characterizing input principal modes in optically scattering medium, Opt. Express 24 (2016) 27691–27701.
[19] S. Bandyopadhyay, P.O. Boykin, V. Roychowdhury, F. Vatan, A new proof for the existence of mutually unbiased bases, Algorithmica 34 (2002) 512–528.
[20] C.A. Fuchs, M.C. Hoang, B.C. Stacey, The SIC question: History and state of play, Axioms 6 (2017) 21.